Binary icosahedral clusters of hard spheres in spherical confinement

Reference:

Wang Da, Dasgupta Tonnishtha, van der Wee Ernest B., Zanaga Daniele, Altantzis Thomas, Wu Yaoting, Coli Gabriele M., Murray Christopher B., Bals Sara, Dijkstra Marjolein, ...- Binary icosahedral clusters of hard spheres in spherical confinement
Nature physics - ISSN 1745-2473 - London, Nature publishing group, 2020, p. 1-9
Full text (Publisher's DOI): https://doi.org/10.1038/S41567-020-1003-9
To cite this reference: https://hdl.handle.net/10067/1720440151162165141

Binary icosahedral clusters of hard spheres in spherical confinement

Da Wang[1,‖,†], Tonnishtha Dasgupta[1,‖], Ernest B. van der Wee[1,‖,‡], Daniele Zanaga[2], Thomas Altantzis[2], Yaoting Wu[3], Gabriele M. Coli[1], Christopher B. Murray[3,4], Sara Bals[2], Marjolein Dijkstra[1,*], and Alfons van Blaaderen[1,*]

[1] *Soft Condensed Matter, Debye Institute for Nanomaterials Science, Utrecht University, Princetonplein 5, 3584 CC, Utrecht, The Netherlands.*

[2] *Electron Microscopy for Materials Science (EMAT), University of Antwerp, Groenenborgerlaan 171, 2020 Antwerp, Belgium.*

[3] *Department of Chemistry, University of Pennsylvania, Philadelphia, PA 19104, United States.*

[4] *Department of Materials Science and Engineering, University of Pennsylvania, Philadelphia, PA 19104, United States.*

[‖] *These authors contributed equally to this work.*

[†] *Present address: Electron Microscopy for Materials Science (EMAT), University of Antwerp, Groenenborgerlaan 171, 2020 Antwerp, Belgium.*

[‡] *Present address: Department of Physics & Astronomy, Northwestern University, Evanston, IL 60208, United States.*

[*] *e-mail: m.dijkstra@uu.nl; a.vanblaaderen@uu.nl*

The influence of geometry on the local and global packing of particles is important to many fundamental and applied research themes such as the structure and stability of liquids, crystals and glasses. Here, we show by experiments and simulations that a binary mixture of hard-sphere-like nanoparticles crystallizing into a $\mathbf{MgZn_2}$ Laves phase in bulk, spontaneously forms icosahedral clusters in slowly drying droplets. Using advanced electron tomography, we are able to obtain the real-space coordinates of all the spheres in the icosahedral clusters of up to about 10,000 particles. The local structure of 70-80% of the particles became similar to that of the $\mathbf{MgCu_2}$ Laves phase. These observations are significant for photonic applications. In addition we observed in simulations that the icosahedral clusters nucleated away from the spherical boundary, which is distinctly different from that of the single species clusters. Our findings open the way for particle-level studies of nucleation and growth of icosahedral clusters, and of binary crystallization.

Crystallization experiments in which droplets were used have contributed significantly to our current understanding on structural aspects and the kinetics of phase transformations in condensed matter physics. Over half a century ago, Turnbull *et al.* showed in seminal experiments that liquids could be undercooled by as much as hundreds degrees below the freezing temperature if they were dispersed as small droplets.[1] The small size of the droplets ensured the absence of heterogeneous nucleation sites, and as a consequence nucleation could only occur homogeneously. The large undercoolings demonstrated that the local structure of liquids differs substantially from that of crystals. These findings inspired Frank to hypothesise that the short-range order in simple liquids has icosahedral symmetry, which is incompatible with the long-range translational order of crystals.[2] The icosahedral order arises locally when one maximises the density, using the convex hull, of a packing of 12 identical spheres on the surface of a central sphere with the same size.[3] The densest packing is obtained by arranging the outer spheres on the vertices of an icosahedron, rather than by using 13-sphere subunits of face-centered cubic (FCC) and hexagonal close-packed (HCP) bulk crystals, which are known to closely pack 3D space at ∼74%.[4–6]

Colloidal suspensions are widely used as model systems to study fundamental processes such as crystallization, melting, nucleation, and the glass transition.[7–11] This is because they have a well-defined thermodynamic temperature, and consequently they display a phase behaviour similar to atoms and molecules. Additionally, they can be investigated on a single-particle level, even in concentrated systems.[7–11] The use of droplets has also been of interest in the soft-matter field, not only because it is a powerful method to study protein crystallization, topological defects in liquid crystal droplets, and the crystallization kinetics of colloids,[10,11] but also to fabricate clusters of particles composed of smaller particles, also termed 'supraparticles' (SPs), upon drying the droplets.[12,13] An unexpected and recent finding in both experiments and simulations is that when up to 90,000 hard spheres (HSs) are compressed under the spherical confinement of a slowly drying emulsion droplet, rather than forming the thermodynamically stable FCC bulk crystal, the system spontaneously crystallizes into icosahedral clusters made up of 20 slightly distorted FCC ordered tetrahedral domains.[14] Using crystallization in spherical confinement, icosahedral clusters were obtained for a range of particle systems.[15–19] Free-energy calculations on pure HSs confined in a spherical confinement showed that clusters with an icosahedral symmetry are thermodynamically more stable than FCC clusters at packing fractions just above freezing.[14] This immediately sets up a highly interesting question for binary HS mixtures which yield stable Laves phases.[20–22]

There are three thermodynamically competing Laves phases:[22] the hexagonal $MgZn_2$, cubic $MgCu_2$, and hexagonal $MgNi_2$ structures.[20,21] The $MgCu_2$ structure is highly appealing for photonic applications because the $MgCu_2$ structure consists of a diamond crystal of large spheres and a pyrochlore lattice of small spheres, which are both substructures displaying a photonic band gap.[23] It is however non-trivial to obtain the $MgCu_2$ structure because the $MgZn_2$ phase was found to be the thermodynamically stable structure in bulk for a binary HS mixture with a diameter ratio in the range of 0.76-0.84, although the free-energy difference between the three Laves phases is small ($\sim 10^{-3}$ k_BT per particle at freezing).[22,23] In light of the recent finding of icosahedral clusters in shrinking droplets of pure HSs,[14] the question becomes whether spherical confinement is also able to stabilise icosahedral clusters with the *cubic* $MgCu_2$ in the tetrahedral wedges, over the bulk stable Laves phase, in binary HSs.

Here we demonstrate, by experiments and simulations, that spherical confinement of a slowly drying emulsion droplet transforms a binary mixture of hard-sphere-like (HS-like) colloids with a size ratio of 0.78, which crystallizes into a structure analogous to the hexagonal $MgZn_2$ Laves phase in bulk, into a binary icosahedral cluster of at least 10,000 particles composed of tetrahedral domains with $MgCu_2$-like structure. In addition, we studied the nucleation and growth of the binary icosahedral clusters by computer simulations and found a nucleation mechanism that is distinctly different from that of the single species clusters.[14]

Self-assembly of binary nanocrystals in spherical confinement

The Laves phases (LS_2)[20,21] are three closely related structures composed of small (S) and large (L) spheres as illustrated in Figs. 1a-c: the hexagonal C14 $MgZn_2$ structure, the cubic C15 $MgCu_2$ structure and the hexagonal C36 $MgNi_2$ structure. The three structures can also be identified by the stacking sequence of the L spheres as viewed along the $[11\bar{2}0]$ or [110] projections of the hexagonal or cubic structures, respectively (Figs. 1d-f).[23] Specifically, the stacking of the L sphere-dimers in the C14, C15, and C36 structures is ...$AABB$..., ...$AABBCC$..., and ...$AABBAACC$..., respectively.[23]

To study the behaviour of a binary nanocrystal (NC) suspension in spherical confinement, we synthesised monodisperse CdSe NCs (S) with a total diameter of 7.7 nm including ligands and monodisperse PbSe NCs (L) with a total diameter of 9.9 nm including ligands (Figs. 1g-h; Supplementary Figs. 1a-b), yielding a binary NC mixture with a diameter ratio of 0.78. To investigate the bulk phase behaviour of the binary NC suspension, the mixture was allowed to self-assemble on a diethylene glycol surface according to a well-developed liquid-air interface method.[24] The Fourier Transform (FT) (Fig. 1i inset) of the transmission electron microscopy (TEM) image of the self-assembled binary NC superlattices (Fig. 1i and Supplementary Fig. 2) shows hexagonal order, corresponding to the [0001] projection of the $MgZn_2$ structure (Fig. 1j). We refer the reader to the Supplementary Information for more details on the $MgZn_2$ identification.

Subsequently, we let the mixture of NCs with a 1:2 number ratio (L:S) self-assemble in slowly drying emulsion droplets,[14] and investigated the structure of the self-assembled SPs using high angle annular dark-field scanning transmission electron microscopy (HAADF-STEM). We found that about 80% of our SPs containing a few hundred up to tens of thousands of NCs show five-fold symmetry, pointing to possible icosahedral ordering (Figs. 2a,e-i; Supplementary Figs. 3-4). However, since HAADF-STEM images only correspond to a 2 dimensional (2D) projection of a 3D object, we performed electron tomography[25,26] to analyse the 3D structure of 6 SPs of different sizes (Figs. 2a,e-i (left column); Supplementary Videos 1 and 3). By using an advanced tomographic reconstruction algorithm,[27] recently developed for quantitative analysis of assemblies of spherical nanoparticles, we obtained coordinates of all particles and identified both the S and L species in the 6 SPs (Figs. 2b-d and e-i (right column); Supplementary Figs. 5-6; Supplementary Videos 2 and 4). As will be detailed in the next section, we confirmed the presence of binary icosahedral clusters in all SPs which exhibited five-fold symmetry.

We also observed a compositional dependence in the influence of the spherical confinement on the self-assembled structure. We found that when the number ratio of the binary mixture corresponds to an excess of S spheres compared to the stoichiometry of the Laves phase, the NCs self-assembled into a $MgZn_2$ crystal structure (similar to the bulk structure) in the SPs as visible in 2D HAADF-STEM images, not yielding five-fold symmetry (Supplementary Fig. 7). However, a NC mixture composition close to the Laves phase stoichiometry yielded icosahedral clusters exhibiting five-fold symmetry. There are only a few papers on binary SPs.[12,16,28–31] Only one of them presents $MgZn_2$-type binary crystals,[16] but they concluded that spherical confinement does *not* change the structure of the binary SPs.

We corroborated our experimental findings with molecular dynamics (MD) simulations, using HOOMD-blue.[32,33] We simulated a binary mixture of N_{tot} = 3,501, 5,001 and 10,002 spheres with a diameter ratio of 0.78 and 1:2

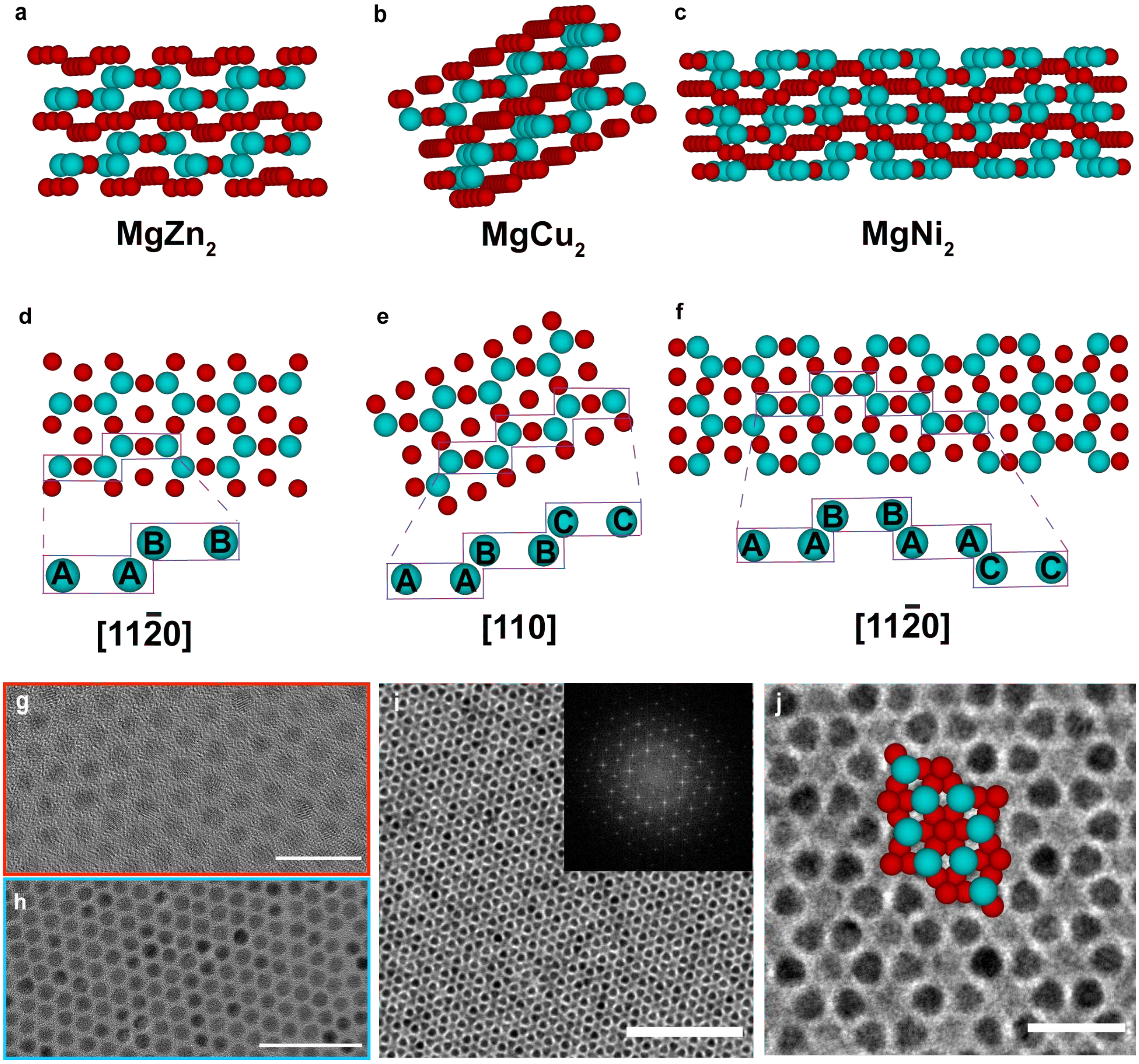

Figure 1: Binary Laves crystal structures. 3D views of the a) C14 ($MgZn_2$), b) C15 ($MgCu_2$) and c) C36 ($MgNi_2$) structures. d) C14 structure viewed along the $[11\bar{2}0]$ projection. e) C15 structure viewed along the [110] projection. f) C36 structure viewed along the $[11\bar{2}0]$ projection. Transmission electron microscopy (TEM) images of g) S CdSe nanocrystals (NCs), h) L PbSe NCs and i-j) binary NC superlattice composed of CdSe and PbSe NCs with a number ratio of $N_S : N_L = 2 : 1$ showing a $MgZn_2$-like structure viewed along the [0001] projection at different magnifications. Fourier transform (FT) of the entire image (inset in i) with a $MgZn_2$ structure model (overlay in j) viewed along the [0001] projection, showing hexagonal symmetry. L and S spheres are coloured in cyan and red, respectively. Scale bars, g-j): 20 nm, 50 nm, 100 nm and 20 nm, respectively. For interactive 3D views of the three Laves phases, see Supplementary Data 1-3.

(L:S) composition interacting with a HS-like potential under spherical confinement (Supplementary Fig. 8) and observed binary icosahedral clusters for all these system sizes, thus indicating that a crossover to the $MgZn_2$ crystal phase requires a bigger system size. This expectation is in line with the observed structural crossover, observed in monodisperse HSs, from (surface-reconstructed) icosahedral clusters to FCC ordering (which is the stable phase in bulk) at a system size of about 90,000 HSs.[14] Our simulations were performed in a fixed spherical volume to speed up equilibration. The overall number densities, and the corresponding *effective* densities for an equivalent binary HS mixture with a diameter ratio of 0.78, are presented in the Methods and Supplementary Methods Section. The striking

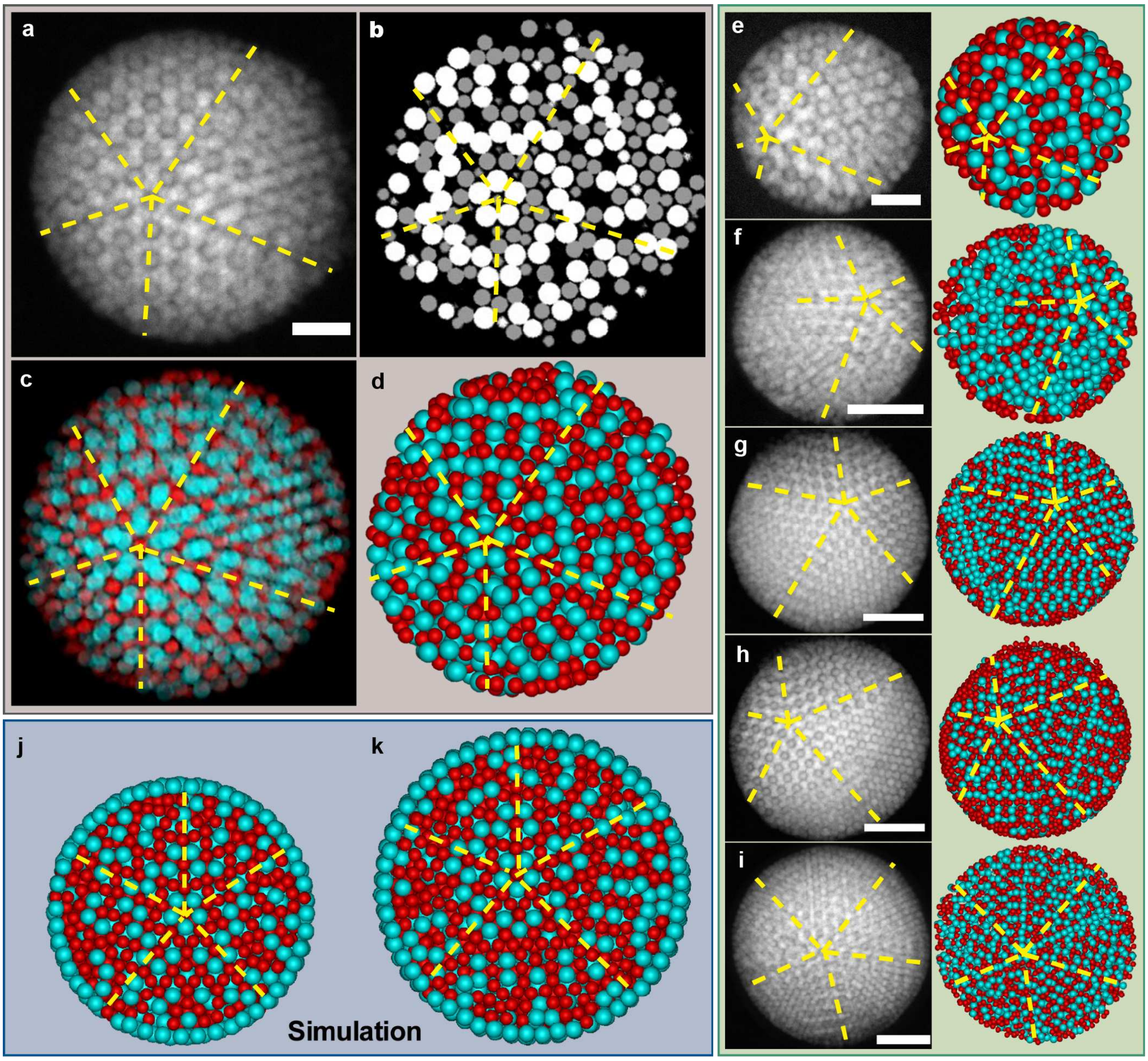

Figure 2: Binary supraparticles (SPs) as obtained from experiments and computer simulations. a) HAADF-STEM image of a typical experimental SP with a diameter of 110 nm containing CdSe/PbSe binary NCs. Corresponding b) reconstructed orthoslice, c) 3D representation and d) cross-section view of the SP in a. Electron tomography of SPs with diameters of e) 80 nm, f) 132 nm, g) 167 nm, h) 170 nm and i) 187 nm, respectively. HAADF-STEM images (left column) and cross-section views (right column) of the binary SPs. Cross-section views of simulated SPs of j) N_{tot} = 3,501 and k) N_{tot} = 5,001 HS-like particles. Five-fold symmetry is visible in both the experimental and simulated SPs, as indicated by the yellow dashed lines. L PbSe and S CdSe NCs are coloured with cyan and red, respectively. Scale bars, a-e) 20 nm and f-i) 50 nm. For an interactive 3D view and more details, see Supplementary Data 4 and 5, Supplementary Tables 1 and 2, respectively.

agreement between the experimental and simulated SPs with regard to the observation of five-fold symmetry is shown in Fig. 2.

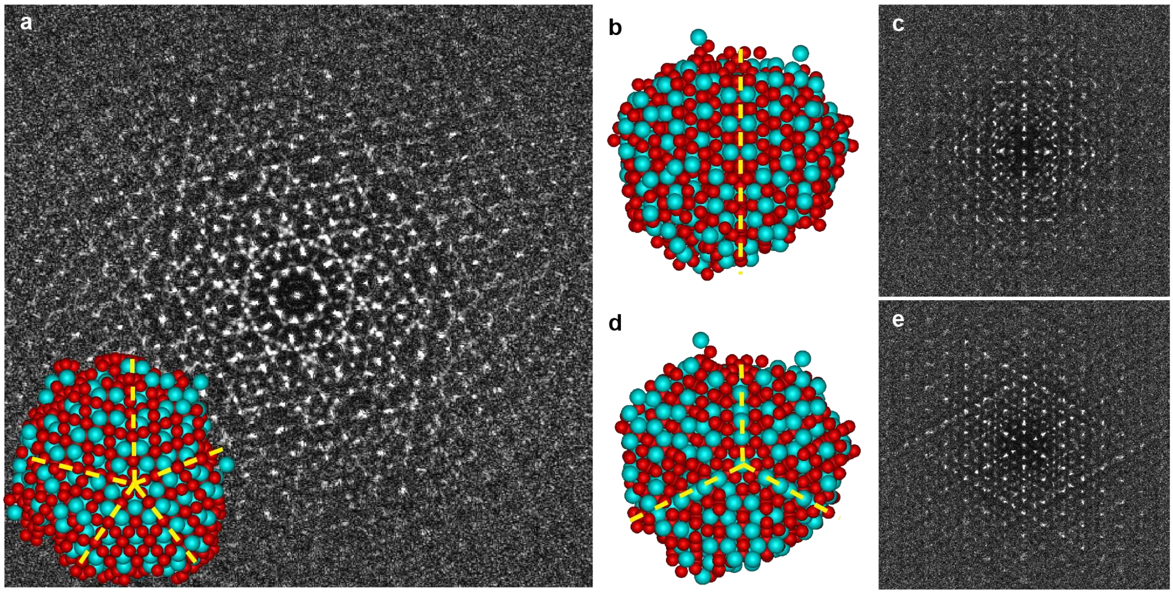

Figure 3: Diffraction pattern of a simulated binary icosahedral SP. a) Diffraction pattern of a simulated binary SP containing N_{tot} = 5,001 particles, showing five-fold orientational symmetry (inset of Fig. 3a). b,d) Real-space configurations of the same SP and c,e) corresponding diffraction patterns viewed along two- and three-fold axes. The diffraction patterns were calculated from time-averaged coordinates of the particles belonging to the binary icosahedral cluster identified using bond-orientational order parameters (BOPs) as described in Supplementary Methods. The particle coordinates were time-averaged over 10,000 configurations.

Fourier-space analysis of binary icosahedral clusters

We calculated diffraction patterns of an experimental SP, which were determined by calculating the FTs of 2D projections of the coordinates (Supplementary Fig. 9). Next, we calculated diffraction patterns of data sets corresponding to a simulated SP (N_{tot} = 5,001; Fig. 3) using the same method, but we averaged the coordinates over a relatively long time, and only selected the particles belonging to the binary icosahedral cluster according to criteria based on bond-orientational order parameters (BOPs; see Methods and Supplementary Methods Section). The sharp Bragg peaks exhibit five-fold (Fig. 3a) as well as two-fold (Figs. 3b-c) and three-fold (Figs. 3d-e) orientational symmetries. This signifies that our SP structure is indeed an icosahedral cluster. As the averaging of the coordinates is not applicable to the experimental data set, the calculated diffraction pattern does not show many higher order Bragg peaks (Supplementary Fig. 9). However, as will be detailed in the next section, the SPs obtained from experiments and simulations were found to have the same structure in real space.

Real-space analysis of binary icosahedral clusters

We found that both our experimental and simulated SPs contained concentric shells with regular polygonic shapes of either S or L particles around a center of symmetry (Figs. 4a-c), which is not positioned at the center of the spherical confinement. These polygonic clusters can be classified as Bergman clusters.[34] The experimental and simulated SPs show striking structural similarity (Fig. 4).

In addition, we analysed the local structural environment of the particles in the SPs using a BOP analysis[35] on the L particles only. Interestingly, the BOPs of the L particles in the binary icosahedral cluster coincide with the BOP

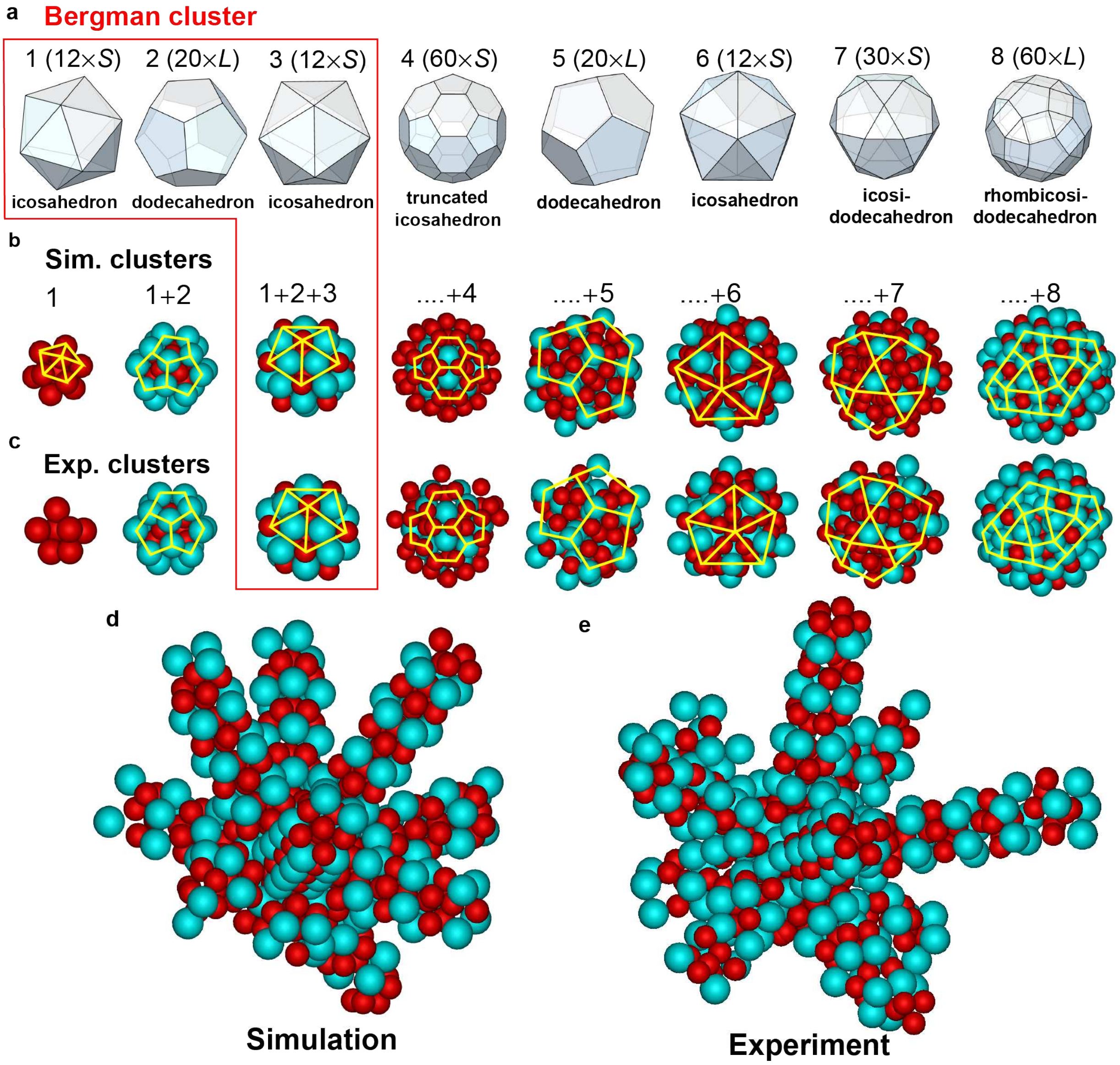

Figure 4: Real-space structure of the binary icosahedral cluster. Binary icosahedral clusters contain concentric shells around the center of symmetry with geometries corresponding to Platonic and Archimedean solids. a) The regular polygons describing the shells up to the 8th shell and the number of particles (of L or S species) forming them. Corresponding regular shells as found in b) simulations and c) experiments, where L and S spheres are coloured in cyan and red, respectively. The yellow lines denote the regular polygons corresponding to the surface tiling of the geometric solids. The 44-particle cluster up to the 3rd shell, as delineated by the red box, corresponds to the Bergman cluster. Along the five-fold symmetry axes of the icosahedral cluster, pentagonal tubes composed of alternating pentagons of L and S particles were found in both d) simulations and e) experiments, all converging at the center of a Bergman cluster. Interactive 3D views (b to e) can be found in Supplementary Data 6 to 9.

signatures of the L particles in both equilibrated $MgZn_2$ and $MgCu_2$ Laves phases in bulk (Supplementary Fig. 10). We present typical configurations of experimental and simulated binary icosahedral clusters, in which the L particles are coloured according to their different BOP values (Supplementary Figs. 11a-d). We observe that the binary icosahedral clusters consist of twenty tetrahedral domains (or wedges) that predominantly consist of particles with a $MgCu_2$-like symmetry, whereas the *shared faces* of adjacent tetrahedral domains are $MgZn_2$-like (Supplementary Figs. 11b,d). Based on single-particle systems, where the tetrahedral domains of the icosahedral clusters were found to be (cubic) FCC-like,[14] it is not surprising that the wedges of our icosahedral SP structures follow a cubic $MgCu_2$-like symmetry. Therefore, the hexagonal $MgZn_2$ Laves phase which is obtained in bulk has been transformed into a SP comprised of domains with a local structure similar to the cubic $MgCu_2$ Laves phase. We further estimated the fraction of $MgCu_2$-like particles in experimental and simulated SPs, for different SP sizes. We see that the spherical confinement forces the local structure of 70-80% of the particles in the SP to resemble that of the $MgCu_2$ Laves phase (Supplementary Fig. 12). In addition, the *edges* of five neighbouring tetrahedral domains form a pentagonal tube (or icosahedral chain[36]) that originates from the Bergman cluster, runs through the whole SP, and ends at one of the twelve vertices with five-fold symmetry on the surface of the SP (Figs. 4d and e). We remark that the pentagonal tubes differ in length as all the Bergman clusters that were found were eccentric with respect to the spherical confinement.

We thus find that a binary mixture of HS-like particles, that crystallizes into the $MgZn_2$ Laves phase in bulk, forms an icosahedral cluster composed of tetrahedral domains with $MgCu_2$-like structure induced by a spherical confinement. It is also worthwhile to highlight that a self-assembled $MgZn_2$ structure (in bulk or in a core-shell SP) would in all probability contain stacking faults as a consequence of minute free-energy differences between the three Laves phases, structurally manifesting from stacking degeneracies along certain planes (Figs. 1d-f) of the crystal structure during nucleation. However, the icosahedral cluster forming under spherical confinement automatically circumvents such stacking faults by enforcing the $MgCu_2$-like structure in the wedges because only the $MgCu_2$-stacking fits the tetrahedral geometry.

Nucleation and growth of binary icosahedral clusters

Now that we have established that the structure of our SPs corresponds to a binary icosahedral cluster, we investigated the mechanism of the binary icosahedral cluster formation, namely, how do these binary icosahedral clusters nucleate and grow? Does our binary icosahedral cluster nucleate from a Bergman cluster and grow shell-by-shell? Or does crystallization start at the spherical interface similar to the formation of icosahedral clusters from single-component HSs in spherical confinement[14]? To study the nucleation and growth of binary icosahedral clusters from a supersaturated binary fluid phase, we used a BOP-based criterion to identify and track the crystal nucleation in our simulations inside a spherical confinement at fixed volume. In Fig. 5a, we plot the fraction of crystalline particles as a function of the radial distance from the center of a SP consisting of $N_{tot} = 5{,}001$ particles at different times along with corresponding typical configurations (Figs. 5b-g). The solid lines denote the crystalline fraction of L spheres while the dashed lines represent the crystalline fraction of the S spheres. The evolution of the structure within the SP shows all the characteristics of nucleation and growth (Figs. 5b-g; Supplementary Video 5). We find that the system remains for a long time in the supersaturated fluid phase, in which small crystalline clusters form and melt in subsequent frames in the spherical confinement (Fig. 5c). At longer times, a single primary cluster nucleates at an off-centered position and starts to grow (Fig. 5d). The nucleus diffuses slightly towards the center of the spherical confinement and grows into the surrounding fluid with time (Figs. 5e-g). This can also be appreciated from Fig. 5a that shows that the crystallization front has grown radially outward with time. We therefore conclude that the binary icosahedral cluster nucleates far away from the spherical boundary. In addition, we find that first a pentagonal tube is formed from which the structure grows out. The growth is therefore not initiated by the Bergman cluster.

An intriguing question is why a mixture that crystallizes into the $MgZn_2$ Laves phase in bulk forms a binary icosahedral cluster under spherical confinement. As the binary icosahedral cluster forms *via* nucleation away from the spherical confinement, the curvature can only be communicated *via* the supersaturated fluid phase. We measured the radial density profiles of the L and S species in the SP at different times in our simulations and found that the density profiles display pronounced layering of particles in concentric shells, which lends strong support to the formation of the binary icosahedral cluster being driven by the structural correlations induced by the spherical curvature in the fluid phase (Supplementary Fig. 13).

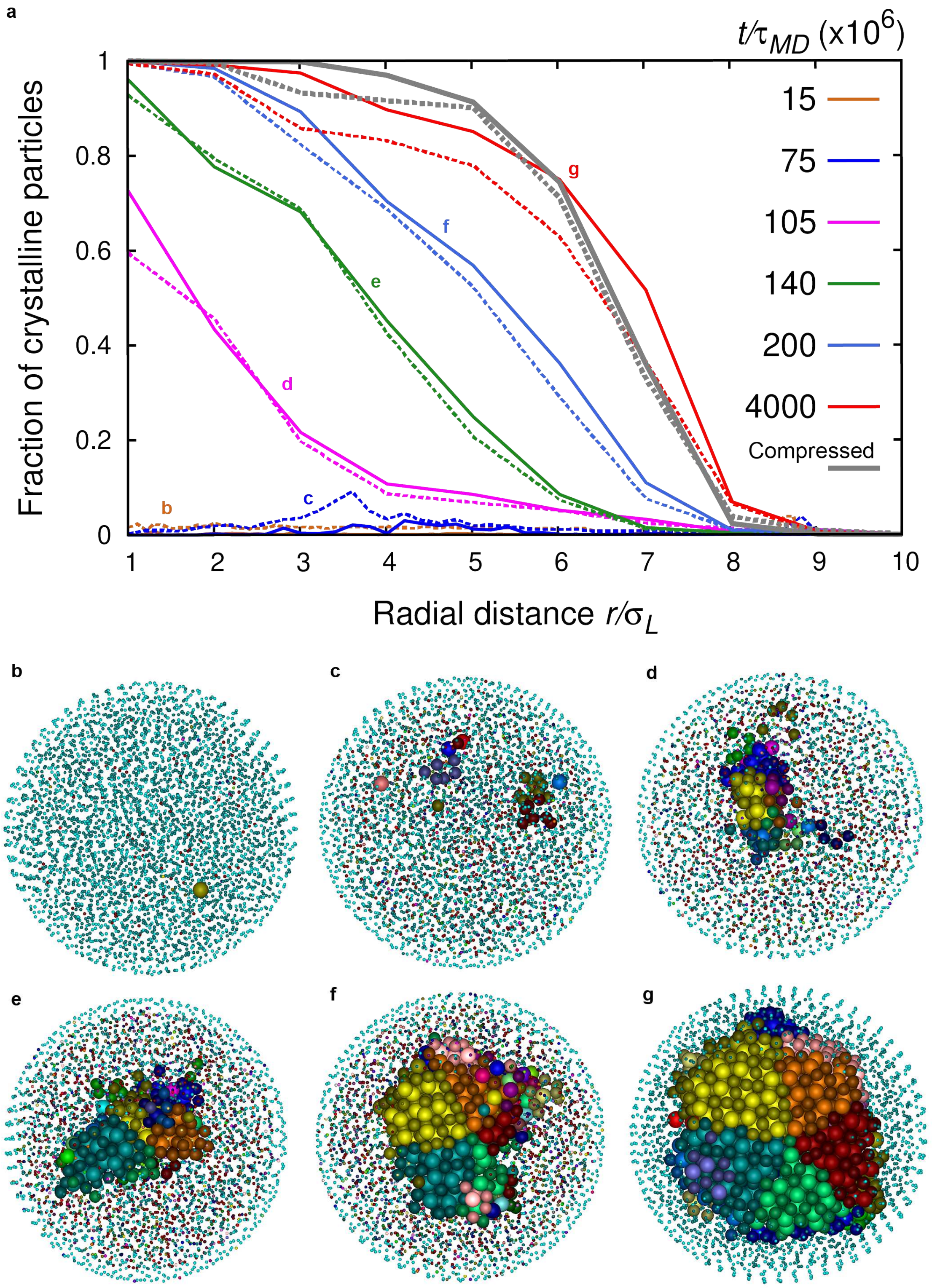

Figure 5: Nucleation and growth of the binary icosahedral cluster in simulations. a) The fraction of crystalline particles as a function of the radial distance from the center of the SP with $N_{tot} = 5{,}001$ particles at different MD times. Crystalline particles belonging to the binary icosahedral cluster are identified using BOPs. The solid and dashed lines denote the crystalline fraction of L and S species, respectively. The crystalline fraction is calculated over the total number of particles of the same species and averaged over 1,000 configurations. The profile shows that the crystal nucleates at an off-centered position and grows radially outward with time. b-g): Typical configurations corresponding to the crystallization profiles shown in a. The labels (b to g) are next to and in the same colour as the corresponding crystallization profiles. The different crystalline domains are shown in different colours. For details on the classification of crystalline domains, see Supplementary Methods Section. The S spheres are coloured in a darker shade of the same colour as the L spheres. Particles not belonging to the binary icosahedral cluster are reduced in size for visual clarity. A video is shown in Supplementary Video 5.

Discussion and conclusion

We demonstrated that a binary mixture of HS-like colloids with a size ratio of 0.78 showing a hexagonal $MgZn_2$ structure in bulk self-assembled into binary icosahedral clusters in slowly drying emulsion droplets. The spherical shape of the SPs allowed a quantitative real-space analysis of the binary icosahedral clusters. The binary icosahedral clusters were found to consist of Bergman clusters with additional concentric shells of particles. In addition, we found that the local structure of the particles in slightly distorted tetrahedral domains of the icosahedral cluster transformed to a $MgCu_2$-like structure. We highlight that the emergence of the $MgCu_2$-like structure is ascribed to the fact that only a cubic $MgCu_2$-like stacking fits the geometry that for the overall cluster ends up being in an icosahedral configuration, alleviating the problems with the degeneracy of the three competing Laves phases. Furthermore, we studied the nucleation and growth mechanism of the binary icosahedral clusters in simulations. We observed that the binary icosahedral clusters nucleated away from the spherical boundary and that the binary icosahedral cluster growth was induced by the pronounced layering of the highly-structured fluid at the spherical boundary. We estimate based on our previous results on the single component SPs[14] and on the qualitative observations of five-fold orientational symmetry in the SPs that also in the binary case the curvature will induce icosahedral symmetry for SPs composed of up to 100,000 particles. The droplet platform as explored here, but using larger colloidal particles that can be imaged in 3D by light nanoscopy, can also be used to obtain the first experimental single particle level information on binary nucleation and growth.

We have shown that the local structure of 70-80% of the particles was changed to $MgCu_2$-like, where the $MgCu_2$ is composed of a cubic diamond lattice of the L spheres and a pyrochlore lattice of the S spheres that both have a photonic band gap for low index contrasts.[22, 23] It would be interesting to investigate both theoretically and experimentally if a photonic band gap can be realised for visible wavelengths in binary icosahedral clusters with $MgCu_2$-like wedges with or without removing one of the sublattices if hard particles with a large index contrast such as titania are used. Although it has recently become possible to grow photonic crystals with diamond sub-structures using DNA interactions,[37, 38] the procedures are complicated and the crystals and index contrasts are not yet good enough to open up photonic band gaps. As our results have been obtained for HS-like particles, it will be straightforward to extend these results to particles with a size closer to the wavelengths of visible light and to particles with a large index contrast such as titania. Moreover, we expect to find the same results for a size ratio range of 0.76-0.84 for which the Laves phases have been shown to be stable.[23] Our finding that binary icosahedral clusters self-assembled from a binary mixture of colloidal HS-like particles in spherical confinement is therefore expected to be interesting for photonic applications.

References

1. Turnbull, D. Phase changes. In *Solid State Physics*, vol. 3, 225–306 (Elsevier, 1956).

2. Frank, F. C. Supercooling of liquids. *Proc. R. Soc. Lond. A* **215**, 43–46 (1952).

3. Taffs, J. & Royall, C. P. The role of fivefold symmetry in suppressing crystallization. *Nat. Commun.* **7**, 13225 (2016).

4. Steinhardt, P. J., Nelson, D. R. & Ronchetti, M. Bond-orientational order in liquids and glasses. *Phys. Rev. B* **28**, 784 (1983).

5. Nelson, D. R. & Spaepen, F. Polytetrahedral order in condensed matter. In *Solid State Physics*, vol. 42, 1–90 (Elsevier, 1989).

6. Spaepen, F. Condensed-matter science: Five-fold symmetry in liquids. *Nature* **408**, 781–782 (2000).

7. Van Blaaderen, A. & Wiltzius, P. Real-space structure of colloidal hard-sphere glasses. *Science* **270**, 1177–1179 (1995).

8. Gasser, U., Weeks, E. R., Schofield, A., Pusey, P. N. & Weitz, D. A. Real-space imaging of nucleation and growth in colloidal crystallization. *Science* **292**, 258–262 (2001).

9. Kegel, W. K. & van Blaaderen, A. Direct observation of dynamical heterogeneities in colloidal hard-sphere suspensions. *Science* **287**, 290–293 (2000).

10. Cheng, Z. *Colloidal Crystallization*, chap. 12, 203–248 (John Wiley & Sons, Ltd, 2016).

11. Fernandez-Nieves, A. & Puertas, A. M. *Fluids, Colloids and Soft Materials: An Introduction to Soft Matter Physics*, vol. 7 (John Wiley & Sons, 2016).

12. Wintzheimer, S. *et al.* Supraparticles: functionality from uniform structural motifs. *ACS Nano* **12**, 5093–5120 (2018).

13. Wang, T., LaMontagne, D., Lynch, J., Zhuang, J. & Cao, Y. C. Colloidal superparticles from nanoparticle assembly. *Chem. Soc. Rev.* **42**, 2804–2823 (2013).

14. De Nijs, B. *et al.* Entropy-driven formation of large icosahedral colloidal clusters by spherical confinement. *Nat. Mater.* **14**, 56–60 (2015).

15. Lacava, J., Born, P. & Kraus, T. Nanoparticle clusters with Lennard-Jones geometries. *Nano Lett.* **12**, 3279–3282 (2012).

16. Yang, Y. *et al.* Scalable assembly of crystalline binary nanocrystal superparticles and their enhanced magnetic and electrochemical properties. *J. Am. Chem. Soc.* **140**, 15038–15047 (2018).

17. Wang, J. *et al.* Magic number colloidal clusters as minimum free energy structures. *Nat. Commun.* **9**, 5259 (2018).

18. Wang, D. *et al.* Interplay between spherical confinement and particle shape on the self-assembly of rounded cubes. *Nat. Commun.* **9**, 2228 (2018).

19. Wang, J. *et al.* Free energy landscape of colloidal clusters in spherical confinement. *ACS Nano* **13**, 9005–9015 (2019).

20. Laves, F. & Witte, H. Der einfluß von valenzelektronen auf die kristallstruktur ternärer magnesiumlegierungen. *Metallw.* **15**, 840–842 (1936).

21. Berry, R. L. & Raynor, G. V. The crystal chemistry of the Laves phases. *Acta Cryst.* **6**, 178–186 (1953).

22. Hynninen, A.-P., Filion, L. & Dijkstra, M. Stability of LS and LS2 crystal structures in binary mixtures of hard and charged spheres. *J. Chem. Phys.* **131**, 064902 (2009).

23. Hynninen, A.-P., Thijssen, J. H. J., Vermolen, E. C. M., Dijkstra, M. & van Blaaderen, A. Self-assembly route for photonic crystals with a bandgap in the visible region. *Nat. Mater.* **6**, 202–205 (2007).

24. Dong, A., Chen, J., Vora, P. M., Kikkawa, J. M. & Murray, C. B. Binary nanocrystal superlattice membranes self-assembled at the liquid-air interface. *Nature* **466**, 474–477 (2010).

25. Saghi, Z. & Midgley, P. A. Electron tomography in the (S)TEM: from nanoscale morphological analysis to 3D atomic imaging. *Annu. Rev. Mater. Res.* **42**, 59–79 (2012).

26. Bals, S., Goris, B., Liz-Marzán, L. M. & Van Tendeloo, G. Three-dimensional characterization of noble-metal nanoparticles and their assemblies by electron tomography. *Angew. Chemie. Int. Ed.* **53**, 10600–10610 (2014).

27. Zanaga, D. *et al.* Quantitative 3D analysis of huge nanoparticle assemblies. *Nanoscale* **8**, 292–299 (2016).

28. Wang, P.-p., Qiao, Q., Zhu, Y. & Ouyang, M. Colloidal binary supracrystals with tunable structural lattices. *J. Am. Chem. Soc.* **140**, 9095–9098 (2018).

29. Chen, O. *et al.* Magneto-fluorescent core-shell supernanoparticles. *Nat. Commun.* **5**, 5093 (2014).

30. Kister, T., Mravlak, M., Schilling, T. & Kraus, T. Pressure-controlled formation of crystalline, Janus, and core-shell supraparticles. *Nanoscale* **8**, 13377–13384 (2016).

31. Yang, Z. *et al.* Supracrystalline colloidal eggs: epitaxial growth and free standing three-dimensional supracrystals in nanoscaled colloidosomes. *J. Am. Chem. Soc.* **138**, 3493–3500 (2016).

32. Anderson, J. A., Lorenz, C. D. & Travesset, A. General purpose molecular dynamics simulations fully implemented on graphics processing units. *J. Comput. Phys.* **227**, 5342 – 5359 (2008).

33. Glaser, J. *et al.* Strong scaling of general-purpose molecular dynamics simulations on GPUs. *Comput. Phys. Commun.* **192**, 97 – 107 (2015).

34. Bergman, G., Waugh, J. L. & Pauling, L. The crystal structure of the metallic phase Mg32 (Al, Zn) 49. *Acta Cryst.* **10**, 254–259 (1957).

35. Lechner, W. & Dellago, C. Accurate determination of crystal structures based on averaged local bond order parameters. *J. Chem. Phys.* **129**, 114707 (2008).

36. Yang, Z. *et al.* Precipitation of binary quasicrystals along dislocations. *Nat. Commun.* **9**, 809 (2018).

37. Ducrot, É., He, M., Yi, G.-R. & Pine, D. J. Colloidal alloys with preassembled clusters and spheres. *Nat. Mater.* **16**, 652–657 (2017).

38. Wang, Y., Jenkins, I. C., McGinley, J. T., Sinno, T. & Crocker, J. C. Colloidal crystals with diamond symmetry at optical lengthscales. *Nat. Commun.* **8**, 14173 (2017).

Methods

Nanocrystal (NC) syntheses 7.7 nm CdSe NCs[39] (a total polydispersity of 2% by counting 130 CdSe NCs; 5.2 nm core diameter) and 9.9 nm PbSe NCs[40] (a total polydispersity of 1% by counting 170 PbSe NCs; 7.6 nm core diameter) were synthesised with minor modifications according to literature methods. This yields a binary NC mixture with a diameter ratio of 0.78. The NC syntheses were carried out in a nitrogen atmosphere using standard Schlenk line techniques. As-synthesised NCs were purified by isopropanol and were dispersed in *n*-hexane with desired weight concentrations. All NCs used in our current work were washed well before self-assembly according to their original experimental protocols. Thus one can assume the amount of free ligands to be negligible after proper washing such that they do not play a significant role during the self-assembly. Our building blocks (cores and ligands) are similar to those used in the work of Evers *et al.*,[41] we therefore describe our experimental system with a hard-sphere-like (HS-like) potential. Detailed information relating to the syntheses can be found in Supplementary Methods Sections 1-2.

Experimental self-assembly of binary NCs in bulk Binary NC superlattices were formed at a liquid-air interface[24] in a glovebox that maintains oxygen- and moisture-free conditions. To prepare a typical $MgZn_2$-type binary NC superlattice, 5.2 nm CdSe and 7.6 nm PbSe NCs were separately dispersed in *n*-hexane at a concentration of 10 mg/mL. Before carrying out the self-assembly, we explored a series of binary mixtures with different number ratios in order to find the optimal conditions to self-assemble $MgZn_2$ bulk structures. The two samples were mixed ($V_{CdSe}/V_{PbSe} \approx 0.9$) to give the right number ratio of NCs ($N_S : N_L = 2 : 1$, matching the stoichiometry of the Laves phases) and form a high-quality $MgZn_2$-type binary NC superlattice film. Then 10 µL of the mixture was dropcasted onto the surface of diethylene glycol in a square Teflon well. A glass slide was placed to cover the well and reduce the evaporation rate of hexane. After 30 minutes, a solid film was obtained on the liquid-air interface. A typical transmission electron microscopy image of the self-assembled binary NC superlattices can be found in Supplementary Fig. 2. Details on the $MgZn_2$ identification can be found in Supplementary Methods Section 3.

Experimental self-assembly of binary NCs in spherical confinement For a typical binary icosahedral cluster assembled from binary NCs in spherical confinement experiment, 6.5 mg of PbSe NCs and 5.85 mg of CdSe NCs were redispersed in 1.0 mL of cyclohexane and added to a mixture of 400 mg of dextran and 70 mg of sodium dodecyl sulfate (SDS) in 10 mL of de-ionized (DI) H_2O. The resulting emulsion was agitated by shear with a shear rate of 1.56×10^5 s^{-1}, using a Couette rotor-stator device (gap spacing 0.100 mm) following the procedure and home-built equipment described by Mason and Bibette.[42] The emulsion was then evaporated at room temperature (RT), while sedimentation was prevented by mixing the emulsion using a VWR VV3 vortex mixer for 48 hours. The resulting supraparticles (SPs) suspension was purified by centrifugation with a speed of 2,500 rpm for 15 minutes using an Eppendorf 5415C centrifuge, followed by re-dispersing in DI H_2O. The aforementioned procedure was repeated twice. The experimental procedure of a typical binary NC self-assembly with an off-stochiometry is similar to that for obtaining the binary icosahedral clusters, except that 6.5 mg PbSe and 6.5 mg CdSe NCs were dispersed in 1.0 mL of cyclohexane and added to a mixture of 400 mg of dextran and 70 mg of SDS in 10 mL of DI H_2O.

Electron microscopy (EM) sample preparation and 2D EM measurements To prepare a sample for conventional EM imaging and electron tomography analysis, 3 µL of the SPs suspension in DI H_2O was deposited on a Quantifoil (2/2, 200 mesh) copper grid and plunge-frozen in liquid ethane using a Vitrobot Mark2 plunge freezer at temperatures around 90 K. The sample was then freeze-dried over a period of 8 hours under vacuum at 177 K and subsequently allowed to warm to RT prior to EM analysis.

Conventional transmission electron microscopy (TEM), 2D high angle annular dark-field-scanning transmission electron microscopy (HAADF-STEM) and 2D energy dispersive X-Ray (EDX) spectroscopy chemical mapping measurements were performed on a FEI-Talos F200X electron microscope, equipped with a high-brightness field emission gun (X-FEG) and operated at 200 kV.

Images and elemental EDX maps were acquired using Bruker Esprit analytical and imaging software in HAADF-STEM mode. Elemental EDX maps of 418×416 pixels were acquired with a 15-minute acquisition time to get a good signal-to-noise ratio, as shown in Supplementary Fig. 7d.

Electron tomography Electron tomography experiments were performed using an aberration-corrected 'cubed' FEI-Titan electron microscope, operated at 300 kV in HAADF-STEM mode. Six electron tomography series of self-assembled binary SPs of different sizes were acquired using a Fischione model 2020 single-tilt tomography holder. For the SPs with a diameter of 80 nm, 110 nm, 132 nm, 167 nm, 170 nm and 187 nm, tilt series were acquired over the following tilt ranges: from -74° to +74°, from -76° to +76°, from -74° to +74°, from -74° to +76°, from -76° to +72° and from -66° to +74°, respectively. The increments in all experiments were set to be 2°.

Tomographic reconstruction Alignment of the tilt series was performed using cross-correlation based routines[43] developed in MATLAB. Tomographic reconstructions were obtained using the Simultaneous Reconstruction Technique (SIRT),[44] as implemented in the ASTRA toolbox, and according to the approach explained in Ref. 27.

The SIRT algorithm was used to obtain a preliminary reconstruction of the tilt series yielding morphological information about the 3D shape of the SP. However, in the presence of close packed particles, conventional SIRT is not sufficient to achieve the reconstruction resolution necessary to segment individual particles and obtain structural information. In order to investigate this in more detail, the Sparse Sphere Reconstruction (SSR) algorithm[27] was used to obtain the coordinates of the particles in the assemblies. The SSR technique has been developed specifically for this purpose. The main idea behind the method is to leverage prior-knowledge in the reconstruction process in order to overcome resolution limitations of SIRT when reconstructing assemblies of close-packed particles. The assumption used is that the particles in the assembly are monodisperse spheres of known size.

In our case the assemblies present two types of particles. However, the particles differ only slightly in size and density, and at the resolutions used for the reconstructions, the difference in size between the two species was less than 2 pixels. Therefore the SSR algorithm could be applied using the approximation of monodisperse particles, and only one size (estimated from the SIRT reconstructions as the size of the smaller species) was used as prior. Once the coordinates of the particles were obtained from the SSR reconstructions, the SIRT reconstruction was used to differentiate the two species which were labelled S species (CdSe NC) and L species (PbSe NC).

To distinguish them, a spherical neighbourhood around each center coordinate and with a radius equivalent to the one of the smaller species (CdSe NCs) was extracted from the SIRT volume. For each point, an average gray value was calculated for these neighbourhoods. Since tilt series were acquired in HAADF-STEM mode, the different atomic numbers of the cations create a different contrast in the SIRT volumes, which yields two different intensity distributions. The intensity distributions were fitted with two Gaussian distributions, and where the intersection of the two curves was taken as the threshold value to distinguish the two species (Supplementary Fig. 5 of the 110 nm binary SP). The overlap of the two curves gives an estimate of the percentage of particles that might be misidentified (*e.g.* $\sim 1\%$ for the 110 nm SP). The 3D representations of all 6 experimental binary SPs from tomographic reconstruction can be found in Figs. 2c,d and e to i (right column).

In order to confirm the validity of the results of the SSR reconstructions, manual segmentation was performed on the SIRT reconstructed volumes of two binary SPs with diameters of 170 nm and 110 nm, respectively, as shown in Supplementary Fig. 6. Due to the smaller size of the CdSe NCs and the lower contrast that exhibited in the SIRT reconstructions compared to the PbSe NCs, manual segmentation of CdSe NCs is time-consuming and far from straightforward. Therefore, we implemented the approach only on the L PbSe NCs. 2,825 and 990 PbSe NCs were detected from the 170 nm SP and 110 nm SP, respectively. The number of PbSe NCs obtained from the SSR reconstructed volumes of the 170 nm and 110 nm SP is 2,814 and 982, respectively. The deviation of the number of the PbSe NCs that obtained from SSR and SIRT is only 0.39% and 0.8% for the 170 nm SP and 110 nm SP, respectively.

Computer simulations We study the spontaneous nucleation of the binary icosahedral clusters by performing molecular dynamics (MD) simulations of a binary mixture of particles inside a spherical confinement, interacting *via* the Weeks-Chandler-Andersen (WCA) pair potential

$$\begin{aligned}\phi_{\alpha\beta}\left(r_{ij}\right) &= 4\epsilon_{\alpha\beta}\left[\left(\frac{\sigma_{\alpha\beta}}{r_{ij}}\right)^{12}-\left(\frac{\sigma_{\alpha\beta}}{r_{ij}}\right)^{6}+\frac{1}{4}\right] && r_{ij}<2^{1/6}\sigma_{\alpha\beta}\\ &=0 && r_{ij}\geq 2^{1/6}\sigma_{\alpha\beta},\end{aligned}$$

where i,j are the interacting particles, α,β denote the particle type (*i.e.* L,S). For our binary mixture, interaction strength $\epsilon_{LL}=\epsilon_{SS}=\epsilon_{LS}=\epsilon$, $\sigma_{LL}\equiv\sigma_L$, $\sigma_{SS}\equiv\sigma_S$, diameter ratio $q=\sigma_S/\sigma_L=0.78$ with $\sigma_{LS}=\left(\sigma_L+\sigma_S\right)/2$, and reduced temperature $T^*=k_BT/\epsilon=0.2$. The WCA potential is short-ranged, steeply repulsive and reduces to the hard-sphere pair potential in the limit of $T^*\to 0$. The interaction potential of the particles with the spherical wall is also a repulsive WCA potential with $\epsilon_w=\epsilon$ and $\sigma_w=\sigma_L$. The simulations are performed using HOOMD-blue (Highly Optimized Object-oriented Many-particle Dynamics)[32, 33] in the canonical NVT ensemble, where the total number of particles $N_{tot}=N_L+N_S$, temperature T, and the volume V are fixed. The temperature is kept constant *via* the Martyna-Tobias-Klein (MTK)[45] integration of the equations of motion based on the Nosé-Hoover thermostat,[46, 47] with coupling constant $\tau_T=1.0$. The time step is set to $\Delta t=0.01\tau_{MD}$ where $\tau_{MD}=\sigma_L\sqrt{m/\epsilon}$ is the MD time unit. In order to ensure sufficient time for equilibration, the simulations are performed in a constant spherical volume. The binary icosahedral cluster nucleation and growth is tracked using a bond-orientational order parameters (BOP)-based cluster criterion as described in Supplementary Methods Section 5. The crystallized SPs are then subjected to a fast compression up to very high densities so as to arrest the positions of the spheres in the SP. The compressed SP structures are subsequently analysed using BOPs on L-L species correlations, as described in Supplementary Methods Section 4. For a close comparison with the experiments, where five-fold SPs were only observed for compositions close to LS_2, we modulate the composition of our binary mixtures such that the number fraction of L particles $x_L=\frac{N_L}{N_L+N_S}$ is ~ 0.3 in the 'core'. The *core* comprises of the SP *excluding* those particles positioned at a radial distance $> R_{SC}-2\sigma_L$ from the center of the SP, where R_{SC} denotes the radius of the spherical confinement. The effective number of particles in the core is denoted by N while the total number of particles in the SP is denoted by N_{tot}. In this work, we simulate $N_{tot}=$ 3,501, 5,001 and 10,002 spheres, which correspond to an effective number of $N=$ 1,990, 3,060 and 6,870 particles in the core of the SP respectively. The supersaturated reduced densities $\rho\sigma^3_{\text{av}}$ $\left(=\frac{3N_{tot}\sigma_L^3}{4\pi R_{SC}^3}\left(x_L+\left(1-x_L\right)q^3\right)\right)$ for which crystallization is observed in our constant volume simulations lie between 0.802–0.831. These densities are equivalent to effective packing fractions $\eta_{\text{HS, eff}}$ in the range 0.506–0.524 for a binary HS mixture with a diameter ratio $q=0.78$. The effective packing fraction for the binary HS mixture is calculated using an *effective diameter*, which can be estimated from WCA perturbation theory (see Supplementary Methods Section 6 for details).

Calculated diffraction pattern The calculated diffraction pattern of the simulated 5,001-particle SP was calculated from the coordinates of particles belonging to the binary icosahedral cluster after the following treatment: (1) the compressed SP was subjected to an equilibration cycle ($t/\tau_{MD}=10^6$, $\Delta t=10^{-3}\tau_{MD}$) and the particle coordinates were averaged over 10,000 configurations, and (2) the time-averaged coordinates were subsequently run through a cluster criterion based on BOPs, which distinguishes the particles belonging to the binary icosahedral cluster from particles with a different local order, as determined by $d_{6,\alpha\beta}(i,j)$ correlations of the particles with their neighbours. Here, α,β denotes the type of species (*i.e.* L,S) and i,j represents the index of the particle and its neighbour respectively. Next, the coordinates of these particles are projected on a 2D plane and the diffraction pattern is obtained by calculating the FT of the resulting projection. The intensity profile in Fig. 3 was filtered with a 1 pixel Gaussian blur to suppress noise. Further details on the BOP criteria are provided in Supplementary Methods Section 5.

Data availability

Data represented in Figs. 2d, e-i (right panel), j-k, 5a, and Supplementary table 2 are available as Source Data. All other data that support the plots within this paper and other findings of this study are available from the corresponding author upon reasonable request.

Code availability

Computer simulations were performed using HOOMD-blue, available at `http://glotzerlab.engin.umich.edu/hoomd-blue/`.

References

39. Pietryga, J. M. *et al.* Utilizing the lability of lead selenide to produce heterostructured nanocrystals with bright, stable infrared emission. *J. Am. Chem. Soc.* **130**, 4879–4885 (2008).

40. Steckel, J. S., Yen, B. K. H., Oertel, D. C. & Bawendi, M. G. On the mechanism of lead chalcogenide nanocrystal formation. *J. Am. Chem. Soc.* **128**, 13032–13033 (2006).

41. Evers, W. H. *et al.* Entropy-driven formation of binary semiconductor-nanocrystal superlattices. *Nano Lett.* **10**, 4235–4241 (2010).

42. Mason, T. G. & Bibette, J. Shear rupturing of droplets in complex fluids. *Langmuir* **13**, 4600–4613 (1997).

43. Guizar-Sicairos, M., Thurman, S. T. & Fienup, J. R. Efficient subpixel image registration algorithms. *Opt. Lett.* **33**, 156–158 (2008).

44. Gilbert, P. Iterative methods for the three-dimensional reconstruction of an object from projections. *J. Theor. Biol.* **36**, 105–117 (1972).

45. Martyna, G. J., Tobias, D. J. & Klein, M. L. Constant pressure molecular dynamics algorithms. *J. Chem. Phys.* **101**, 4177–4189 (1994).

46. Nosé, S. A unified formulation of the constant temperature molecular dynamics methods. *J. Chem. Phys.* **81**, 511–519 (1984).

47. Hoover, W. G. Canonical dynamics: Equilibrium phase-space distributions. *Phys. Rev. A* **31**, 1695–1697 (1985).

Acknowledgments

D.W., E.B.v.d.W. and A.v.B. acknowledge partial financial support from the European Research Council under the European Union's Seventh Framework Programme (FP-2007–2013)/ERC Advanced Grant Agreement 291667 HierarSACol. T.D. and M.D. acknowledge financial support from the Industrial Partnership Programme, "Computational Sciences for Energy Research" (Grant no. 13CSER025), of the Netherlands Organization for Scientific Research

(NWO), which was co-financed by Shell Global Solutions International B.V. G.M.C. was also financially supported by NWO. S.B. acknowledges financial support from ERC Consolidator Grant No. 815128 REALNANO. T.A. acknowledges a post-doctoral grant from the Research Foundation Flanders (FWO, Belgium). C.B.M and Y.W. acknowledge support for materials synthesis from the Office of Naval Research Multidisciplinary University Research Initiative Award ONR N00014-18-1-2497. G. A. Blab is gratefully acknowledged for 3D printing numerous truncated tetrahedra which increased our understanding of the connection between the binary icosahedral cluster and Laves phase structures. N. Tasios is sincerely thanked for providing the code for the diffraction pattern calculation. M. Hermes is sincerely thanked for providing interactive views of the structures in this work. The authors thank G. van Tendeloo, M. Engel, J. Wang, S. Dussi, L. Filion, E. Boattini, S. Paliwal, N. Tasios, B. van der Meer, I. Lobato, J. Wu and L. Laurens for fruitful discussions. The authors acknowledge the EM square center at Utrecht University for the access to the microscopes.

Author contributions

A.v.B. initiated the investigation of icosahedral order in binary crystals under spherical confinement and supervised D.W. and E.B.v.d.W. M.D. initiated the simulation study on the binary icosahedral clusters in spherical confinement and supervised T.D. and G.M.C. T.D. performed computer simulations of the spontaneous nucleation of binary icosahedral clusters. D.W. synthesised the SPs and obtained, together with T.A., the electron tomography. D.Z. performed SSR tomographic reconstruction and T.A. performed manual segmentations, under the supervision of S.B. Y.W. synthesised NCs under the supervision of C.B.M. E.B.v.d.W., T.D. and G.M.C. developed the BOP analysis of the Laves phases, the binary icosahedral clusters and the cluster criterion to track the nucleation of the binary icosahedral clusters. D.W., T.D., E.B.v.d.W., M.D. and A.v.B. analysed the results. A.v.B., M.D., D.W., T.D. and E.B.v.d.W. co-wrote the manuscript. All authors discussed the text and interpretation of the results.

Additional information

Supplementary information is available in the online version of the paper. Reprints and permissions information is available online. Correspondence and requests for materials should be addressed to M.D. or A.v.B.

Competing interests

The authors declare no competing interests.